Stress Field inside the Bath Determines Dip Coating with Yield-Stress Fluids in Cylindrical Geometry

Wilbert J. Smit[1,*] Christophe Kusina,[1] Jean-François Joanny,[2,3] and Annie Colin[1,4]

[1]Chimie Biologie Innovation, ESPCI Paris, CNRS, PSL University, 10 rue Vauquelin, 75005 Paris, France
[2]Physico Chimie Curie, Institut Curie, PSL University, 26 rue d'Ulm, 75005 Paris, France
[3]Collège de France, 11 place Marcelin Berthelot, 75005 Paris, France
[4]Centre de Recherche Paul Pascal, CNRS, Université de Bordeaux, 115 Avenue Schweitzer, 33600 Pessac, France

We study experimentally and theoretically the thickness of the coating obtained by pulling out a rod from a reservoir of yield-stress fluid. Opposite to Newtonian fluids, the coating thickness for a fluid of large enough yield stress is determined solely by the flow inside the reservoir and not by the flow inside the meniscus. The stress field inside the reservoir determines the thickness of the coating layer. The thickness is observed to increase nonlinearly with the sizes of the rod and of the reservoir. We develop a theoretical framework that describes this behavior and allows us to precisely predict the coating thickness.

Dip coating is a coating technique in which an object is immersed into a fluid reservoir and then pulled out. During the withdrawal, a liquid film is entrained by viscous drag. The dip-coating process is low cost, waste-free, and easy to scale up [1]. Applications are found in many sectors ranging from manufacturing to the food industry and cosmetics [2–4]. Predicting the thickness of the entrained film is of major interest, both from the industrial and scientific perspectives. Since the seminal works by Landau and Levich [5] and Derjaguin [6], the problem has received continuing interest. In the case of Newtonian liquids, the balance between viscosity and surface tension (capillary number) determines the film thickness [7–9]. However, for soft-jamming liquids with a finite yield stress such as paints, gels, pastes, foams, and creams, a complete, self-contained description remains elusive, despite its industrial relevance.

In recent years, the dip coating problem with a yield-stress fluid has been studied both experimentally [10–13] and by numerical simulations [12,14,15]. Maillard et al. have shown that for fluids with a high yield stress viscous dissipation is sufficiently large for the capillary effects to be negligible. In planar geometry, they observed that the coating thickness is determined by a competition between viscous drag and gravity in the meniscus [10–12]. In this work, we revisit the problem by studying the axisymmetric coating problem. We show that the coated thickness results from the exact upward flux of the flowing fluid zone created close to the rod only in the bath. For high yield stress, the thickness is completely determined by the stress field inside the bath and independent on the surface tension. This regime has not been observed previously in planar geometry. The curvature of the geometry is at its origin. It modifies the stress field in the bath and limits the size of

the fluidized zone, canceling the role of the drainage. We develop a semianalytic model that captures this picture quantitatively.

The dip-coating experiments are performed in the axisymmetric geometry, in which a rod is pulled out from the center of a cylindrical container [Fig. 1(a)]. Cylindrical containers of various radii r_2 (13, 17, 21.5, and 33 mm) and height 14 cm. As a model yield-stress fluid, we use Carbopol microgels that have been extensively studied [16–18]. During the preparation, the samples are sheared gently during 2 h. The Carbopol powder is dissolved under gentle stirring for 1 h in pure water, the aqueous Carbopol 980 solutions (0.08–0.5 wt%) are neutralized with a dilute solution of NaOH and the samples are stirred gently for
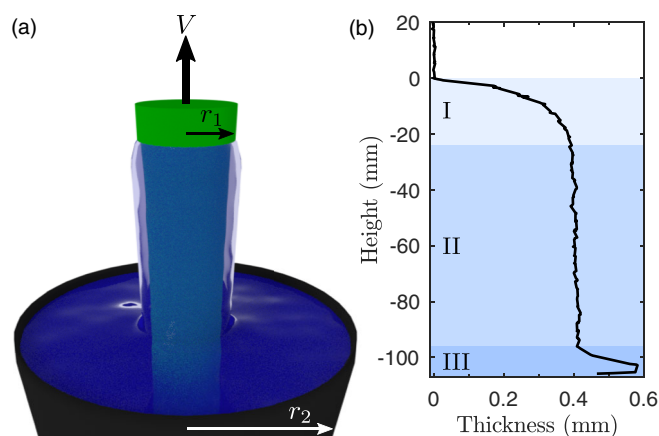
FIG. 1. (a) Schematic of the dip-coating experiment. A rod of radius r_1 is pulled out with velocity V from a liquid bath of radius r_2. (b) Typical thickness profile resulting from the dip coating. The coating profile can be divided into regions I, II, and III (see text).

another 1 h. Bubbles are removed by ultracentrifugation. The gels have a density of 10^3 kg m^{-3}. These gels are model yield-stress system: subjected to an up and down shear rate sweep, they do not exhibit hysteresis. Their flow curve, i.e., shear stress τ vs shear rate $\dot{\gamma}$, is well described by a Herschel-Bulkley model for which $\tau = \tau_c + k\dot{\gamma}^n$ with τ_c the yield stress, k the consistency index, and n the shear-thinning index (see Fig. S1 in the Supplemental Material [19]) [11,20]. The dip-coating experiments are performed with acrylic rods of radius $r_1 = 2.5$–10 mm, which are vertically immersed over a length of 10 cm into the bath. To minimize wall slip [21,22] and to ensure complete wetting of the Carbopol gels on the acrylic rods, the rods are sandblasted leading to a roughness of $\sim$10 μm and subsequently treated by an oxygen-argon plasma (Diener Pico) [23]. The internal stress of the gel in the container is preset by a first immersion and retraction of the rod. The immersion of the rod is performed at the same speed as the retraction. The coating thickness is directly measured using a profilometer (Keyence LJ-V7060K).

A typical thickness profile from a dip-coating experiment is shown in Fig. 1(b). The coating profile can be divided into three parts: In the top region (I), the coating thickness builds up. In the bottom region (III), the thickness increases as a result of the breakage of the meniscus when the rod leaves the liquid bath. In the intermediate region (II), the coating thickness is uniform, which is associated with a steady flow (see discussion below). In this Letter, we focus on region II and denote the constant thickness by h. Its value is determined by averaging over 3–10 independent measurements.

In Fig. 2 we show the experimental film thickness h for a 0.5% Carbopol solution in 1% aqueous PEG-12 dimethicone in several configurations. Using the sessile-drop technique, we measure a surface tension σ of 27 mN m^{-1} for a 1% PEG solution in water. We assume that the surface tension of the Carbopol solution with 1% PEG has the same value. The coating thickness increases with rod radius r_1 as well as with pull-out velocity V, see panels (a) and (b), respectively. Strikingly, the gap width also has a profound impact on the coating thickness. For instance, for a rod of radius $r_1 = 10$ mm, the thickness h increases from 0.35 ± 0.01 mm for $r_2 - r_1 = 7$ mm to 0.68 ± 0.03 mm for $r_2 - r_1 = 23$ mm. This result contrasts the behavior for Newtonian liquids, for which the coating thickness is independent on the bath size when the distance to the wall exceeds 2 times the capillary length in the case of a plate geometry [24]. The dependence on the bath size for a yield-stress fluid implies that the coating does not only induce a flow of a free surface under gravity, but that the coating process is governed by the flow inside the bath.

To solve the dip-coating problem for a yield-stress fluid, we must determine the fluid flow inside the bath. For a laminar flow along the rod away from the meniscus and the end of the rod, the only nonvanishing stress component is
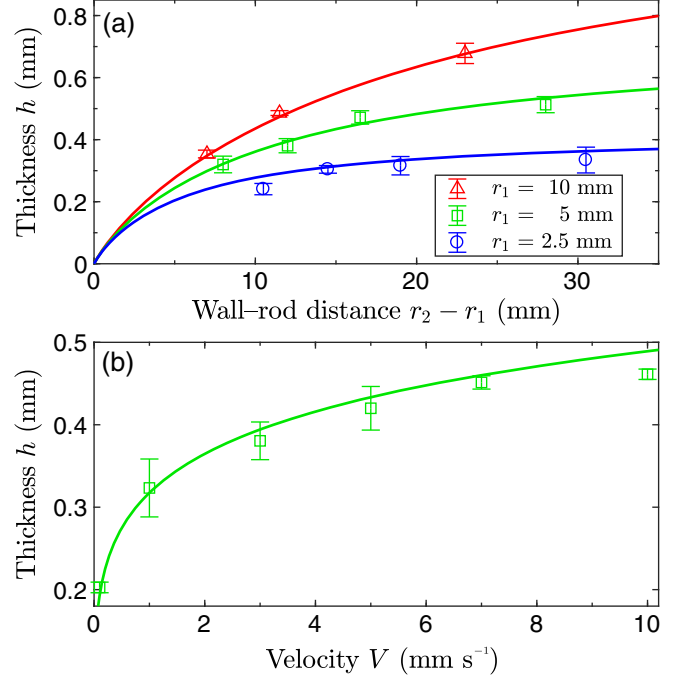
FIG. 2. Comparison of the coating thickness between experiments (data points) and the prediction of Eq. (6) (solid lines) for a Carbopol solution in aqueous PEG-12 dimethicone. The rheological properties are $\tau_c = 54$ Pa, $k = 29$ Pa s^n, and $n = 0.35$. Error bars denote the standard deviation. (a) Coating thickness as a function of the distance between bath wall and rod for different geometrical configurations. The rod radii are 2.5 (circles), 5 (squares), and 10 mm (triangles). The withdrawal velocity is 3 mm s^{-1}. (b) Coating thickness as a function of withdrawal velocities. The rod and the bath are of radius $r_1 = 5$ and $r_2 = 17$ mm, respectively.

the transverse stress τ_{rz}. In our experiments, inertial forces are small compared to viscous forces (Reynolds number < 0.1). Owing to the low value of the Reynolds number, the flow is governed by Stokes' equation,

$$-\rho g - \frac{\partial P}{\partial z} + \frac{1}{r}\frac{\partial r \tau_{rz}}{\partial r} = 0, \tag{1}$$

with fluid density ρ, gravitational acceleration g, pressure P, radial coordinate r, and vertical coordinate z. By integration, a general solution for flow through concentric annuli is obtained:

$$\frac{\tau_{rz}(r)}{\tau_c} = \frac{1}{\lambda_i - \lambda_o}\left(r - \frac{\lambda_i \lambda_o}{r}\right). \tag{2}$$

To be determined are λ_i and λ_o, the locations of the inner and outer yield surfaces, respectively, i.e., $\tau_{rz}(\lambda_i) = -\tau_c$ and $\tau_{rz}(\lambda_o) = \tau_c$. For elastoviscoplastic fluids, λ_i and λ_o depend on the deformation history and converge after a start-up time to their steady flow values [25]. In all our experiments, the rod length is sufficiently long for a steady

flow to be established, as evidenced from the constant region in the coating profiles (region II in Fig. 1) and measurements of the force between rod and reservoir (Fig. S2 [19]). In this case, λ_i and λ_o do not depend upon time and can be determined by assuming no-slip boundary conditions, i.e., $v_z(r_1) = V > 0$ and $v_z(r_2) = 0$, and mass conservation. The velocity boundary conditions impose

$$V + \int_{r_1}^{r_2} \dot{\gamma}(r)\mathrm{d}r = 0, \qquad (3)$$

with shear rate $\dot{\gamma} = \partial v_z/\partial r$. Mass conservation imposes that the retracted volume by the rod pull-out be balanced by a downward flux of the liquid in the bath:

$$2\pi \int_{r_1}^{r_2} rv_z(r)\mathrm{d}r = -\pi r_1^2 V. \qquad (4)$$

To obtain the bath flow, one must specify a rheological model. Here, we employ the Herschel-Bulkley model for which $\dot{\gamma} = 0$ for $\tau \leq \tau_c$ (solid regime) and $\tau = \tau_c + k\dot{\gamma}^n$ for $\tau > \tau_c$ (liquid regime). Using Eq. (2), the shear rate can be expressed as

$$\dot{\gamma}(r) = \begin{cases} -\left(\frac{\tau_c}{k}\right)^{1/n}\left(\frac{\frac{\lambda_i\lambda_o}{r} - r + \lambda_i - \lambda_o}{\lambda_o - \lambda_i}\right)^{1/n} & r_1 \leq r < \lambda_i \\ 0 & \lambda_i \leq r \leq \lambda_o \\ \left(\frac{\tau_c}{k}\right)^{1/n}\left(\frac{r - \frac{\lambda_i\lambda_o}{r} + \lambda_i - \lambda_o}{\lambda_o - \lambda_i}\right)^{1/n} & \lambda_o < r \leq r_2. \end{cases} \qquad (5)$$

Using this expression of the shear rate, we perform a double iteration analogous to Fordham *et al.* [26] to fulfill Eqs. (3) and (4). We obtain the two yield positions λ_i and λ_o. The obtained flow is shown in Fig. 3 and agrees quantitatively with experimental measurements of the velocity profile. The latter have been obtained by seeding a thin slit of the gel with some bubbles and by following their displacement. Two sheared zones close to the rod and the reservoir are clearly evidenced. The displacement of the bubbles shows that there is no horizontal flow at the surface. Only towards the end of the rod, does a horizontal flow bring matter from the sides to fill up the extracted volume below the rod's end [27]. This flow occurs over a characteristic length of $\sim$2–3 cm (a distance comparable to r_2) and does not affect the previously calculated velocity profile.

When one assumes that the fluid in the liquid region between r_1 and λ_i inside the bath is transferred onto the coating with velocity $V - v_z(\lambda_i)$, mass conservation yields a layer of thickness (as derived in Sec. III of Supplemental Material [19])

$$h = -r_1 + \sqrt{\frac{\int_{r_1}^{\lambda_i} r^2 \dot{\gamma}(r)\mathrm{d}r}{\int_{r_1}^{\lambda_i} \dot{\gamma}(r)\mathrm{d}r}}. \qquad (6)$$
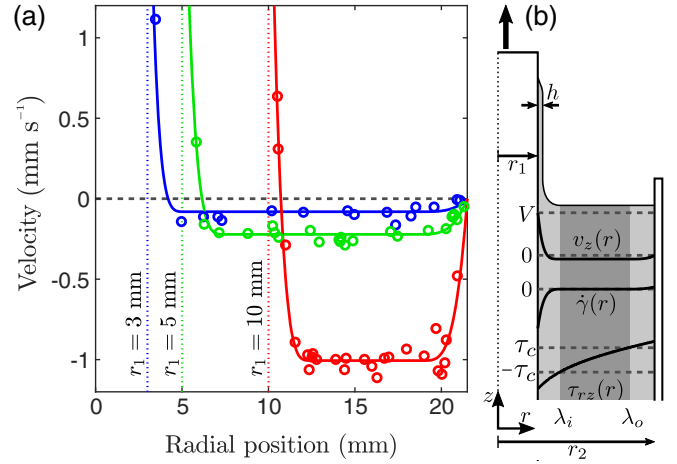
FIG. 3. (a) Velocity profiles for rods of various radii r_1 withdrawn from a bath of $r_2 = 21.5$ mm with velocity 3 mm s^{-1}. The data points are obtained by tracking the flow of small air bubbles inserted perpendicular to the plane of observation. The solid lines result from the velocity and mass-conservation conditions (without fit parameter). The rheological properties of the Carbopol gel are $\tau_c = 14$ Pa, $k = 8$ Pa s^n, and $n = 0.35$. (b) Schematic of flow during the dip-coating experiment. Radial profile of the steady flow inside the bath of the velocity v_z, shear rate $\dot{\gamma}$, and shear stress τ_{rz}. The yielded regions are indicated light-shaded and the unyielded regions are indicated dark-shaded.

In the meniscus region, the fluid turns progressively from a liquid to a solid behavior.

The numerical values of the coating thickness h are plotted as solid lines in Fig. 2 and are in excellent agreement with the experimental results. The influence of the geometrical dimensions as well as the velocity on the coating thickness is well captured by the model. The thickness of the coating layer is most variable when the bath size is small and when the pull-out velocity is low as predicted by the model. Importantly, the flow inside the bath depends on three independent length scales [r_1, r_2, and the rheological length $V(k/\tau_c)^{1/n}$]. Hence, at least two dimensionless parameters are required to describe the flow [e.g., r_2/r_1 and Bingham number Bm $= (\tau_c/k)(r_2 - r_1/V)^n$]. As a consequence, no single master curve for all rod sizes, bath sizes, and velocities can be presented. The quantitative agreement between model and experiment shows that the liquid moved upwards in the bath is completely transferred onto the coating. Our results indicate that both capillary effects and gravity play no role. Let us discuss these hypotheses.

Capillary effects play a role when the stress gradient in the deposit, $\sim\tau_c/h$, is less than the characteristic capillary pressure gradient in the meniscus close to the rod. In our work, the capillary length $l_c = \sqrt{\sigma/\rho g}$ is smaller than or comparable to the radii of the rods and the characteristic capillary pressure gradient is $\sigma/\sqrt{hl_c^3}$ [9]. This means that capillary forces can be neglected for $\tau_c > (\rho g)^{3/4}h^{1/2}\sigma^{1/4}$, which is well-fulfilled for the data in Fig. 2.

Drainage does not affect the coating thickness when the width of the liquid zone around the rod is smaller than the gravity-imposed drainage limit, i.e., $\lambda_i < r_1 \sqrt{1 + 2\tau_c/\rho g r_1}$ [28]. This criterion shows that drainage is negligible for the data in Fig. 2.

We show in Fig. 4 the outcomes of experiments with Carbopol solutions with yield stress of 3, 8, 18, and 28 Pa in neat water, i.e., without PEG-12 dimethicone. The surface tension of these aqueous Carbopol solutions is 63 mN m^{-1} [29]. Our model yields a good agreement with experiment when the yield stress is higher than 18 Pa. In these situations, capillary effects are small. Drainage can be neglected as soon as the yield stress is higher than 8 Pa for $r_1 = 2.5$ mm and higher than 18 Pa for $r_1 = 5$ and 10 mm. For yield-stress values of 3 and 8 Pa, the coating thickness is observed to vary little with bath size and our modeling does not describe the measured values. Capillary effects and drainage both play a role.

The good agreement contrasts the observation by Maillard *et al.*, who found a 40%–60% thinner deposit than the total amount of fluid driven upwards [10,12]. Let us first comment that an implementation of our modeling in planar geometry predicts perfectly and quantitatively both the velocity profiles and the size of the fluidized zone measured in the work of Maillard *et al.* [12] (see Fig. S4 in Ref. [19]). This underlines that our modeling whose

FIG. 4. Transition from the meniscus-shaped regime to the bath-flow regime for dip coating from aqueous Carbopol solutions with increasing yield stress. The experimental data points are compared with the weighted averages per rod size (dashed lines) and/or the bath-flow model (solid lines). The withdrawal velocity is 3 mm s^{-1}. The rheological properties of the Carbopol gels are (a) $\tau_c = 28$ Pa, $k = 14$ Pa s^n, $n = 0.35$. (b) $\tau_c = 18$ Pa, $k = 10$ Pa s^n, $n = 0.35$. (c) $\tau_c = 8$ Pa, $k = 4$ Pa s^n, $n = 0.42$. (d) $\tau_c = 3$ Pa, $k = 1.6$ Pa s^n, $n = 0.47$.

originally is to take into account the boundary conditions and to write a zero-flux condition, captures quantitatively the steady flow in the bath in the low-Reynolds limit. The difference between our study and the work of Maillard *et al.* comes from the role of drainage. As suggested by these authors, gravity and drainage in the meniscus are at the origin of the loss of matter.

One may wonder then, why do the results of Maillard *et al.* differ from ours and why does gravity not interfere in the case of our rods? For a plate geometry, the thickness of the liquid region along the plate λ_i^{plate} is found to diverge as $\lambda_i^{\text{plate}} \propto L^{1/1+n}$, with L the bath size (see Sec. V in Ref. [19]). When the thickness of the liquid zone exceeds a critical value, drainage will occur in the meniscus region. For a plate, drainage likely occurs in the meniscus region, when the thickness of the liquid region along the plate λ_i^{plate} is larger than the drainage limit $\tau_c/\rho g$. In the experiment of Maillard *et al.* wide baths are employed and drainage occurred in the meniscus region as λ_i^{plate} exceeds $\tau_c/\rho g$, due to the scaling of $\lambda_i^{\text{plate}} \propto L^{1/1+n}$.

Conversely for a cylindrical geometry, the location of the inner yield radius λ_i reaches a plateau value when the bath size tends to infinity. The curvature of the rod results in a faster dissipation of the stress field than in the case of a plate in which the stress field is linear [cf. Eqs. (2) and (S15) [19]]. Pulling out a finite rod thus entrains a smaller amount of liquid than pulling out a plate in a wide bath. In the case of more complex geometries, a numerical approach is likely required to obtain the stress field inside the bath from the velocity boundary conditions and mass conservation.

To conclude, let us come back to the steady character of the flow. As pointed out by the measurement of the force on the rod and by the constant coating thickness, our rods are sufficiently long to establish a steady flow. An overestimate of the time needed to reach steady flow can be made by assuming that steady state occurs when the critical strain γ_c is reached at position λ_o, yielding the time $\gamma_c(r_2 - \lambda_o)/V_d$, where V_d is the downward velocity of the fluid. Neglecting the wetting film on the external wall which is much smaller than h, mass conservation gives $V_d = -V(r_1 + h)^2/(r_2^2 - r_1^2)$. The critical strain γ_c required to overcome the yield stress is smaller than 20% in the case of our gels [18]. It follows that the longest transients in our experiments which occur for $r_1 = 2.5$ and $r_2 = 33$ mm are less than the duration of the experiment.

In summary, we have studied the axisymmetric dip-coating problem for a yield-stress fluid. As for Newtonian fluids, we show that geometry plays a critical role. For Newtonian fluids, the shape of the meniscus differs for a plate and for a rod. For yield-stress fluids, the geometry determines the stress field and the amount of fluid in its liquid state.

————————

*wilbert.smit@espci.fr

[1] D. Grosso, J. Mater. Chem. **21**, 17033 (2011).

[2] S. Kalpakjian, K. S. Vijai Sekar, and S. R. Schmid, *Manufacturing Engineering and Technology*, 7th ed. (Pearson, Upper Saddle River, NJ, 2014).

[3] P. Sathish Kumar, R. Rajasekar, S. K. Pal, G. C. Nayak, and S. M. R. Syed Ismail, Paints and coating of multicomponent product, in *Multicomponent Polymeric Materials*, edited by J. K. Kim, S. Thomas, and P. Saha (Springer, Netherlands, Dordrecht, 2016), pp. 157–226.

[4] D. Lin and Y. Zhao, Compr. Rev. Food Sci. Food Saf. **6**, 60 (2007).

[5] L. Landau and B. Levich, Acta Physicochim. URSS **17**, 42 (1942).

[6] B. Derjaguin, C.R. Acad. Sci. URSS **39**, 13 (1943).

[7] D. Quéré, Annu. Rev. Fluid Mech. **31**, 347 (1999).

[8] G. Orsini and V. Tricoli, Phys. Fluids **29**, 052106 (2017).

[9] E. Rio and F. Boulogne, Adv. Colloid Interface Sci. **247**, 100 (2017).

[10] M. Maillard, J. Boujlel, and P. Coussot, Phys. Rev. Lett. **112**, 068304 (2014).

[11] M. Maillard, J. Boujlel, and P. Coussot, J. Non-Newtonian Fluid Mech. **220**, 33 (2015).

[12] M. Maillard, C. Bleyer, A. L. Andrieux, J. Boujlel, and P. Coussot, Phys. Fluids **28**, 053102 (2016).

[13] B. Trottet, M. Marconati, J. L. Keddie, and M. Ramaioli, Chem. Eng. Trans. **57**, 1897 (2017).

[14] A. Filali, L. Khezzar, and E. Mitsoulis, Comput. Fluids **82**, 110 (2013).

[15] J. Bleyer, M. Maillard, P. De Buhan, and P. Coussot, Comput. Methods Appl. Mech. Eng. **283**, 599 (2015).

[16] J. M. Piau, J. Non-Newtonian Fluid Mech. **144**, 1 (2007).

[17] P. Coussot, J. Non-Newtonian Fluid Mech. **211**, 31 (2014).

[18] M. Dinkgreve, M. Fazilati, M. M. Denn, and D. Bonn, J. Rheol. **62**, 773 (2018).

[19] See Supplemental Material at http://link.aps.org/supplemental/10.1103/PhysRevLett.123.148002 for a typical force curve during a dip-coating cycle, a dimensionless description of the model, and the description for a plate.

[20] B. Geraud, L. Bocquet, and C. Barentin, Eur. Phys. J. E **36**, 30 (2013).

[21] P. Coussot, *Rheometry of Pastes, Suspensions, and Granular Materials: Applications in Industry and Environment* (Wiley, New York, 2005).

[22] D. Bonn, M. M. Denn, L. Berthier, T. Divoux, and S. Manneville, Rev. Mod. Phys. **89**, 035005 (2017).

[23] K. Tsougeni, P. S. Petrou, A. Tserepi, S. E. Kakabakos, and E. Gogolides, Microelectron. Eng. **86**, 1424 (2009).

[24] O. Kim and J. Nam, J. Fluid Mech. **827**, 1 (2017).

[25] I. Cheddadi, P. Saramito, and F. Graner, J. Rheol. **56**, 213 (2012).

[26] E. J. Fordham, S. H. Bittleston, and M. A. Tehrani, Ind. Eng. Chem. Res. **30**, 517 (1991).

[27] J. Boujlel, M. Maillard, A. Lindner, G. Ovarlez, X. Chateau, and P. Coussot, J. Rheol. **56**, 1083 (2012).

[28] The critical drainage thickness follows from Eq. (1) in the absence of a pressure gradient ($\partial P/\partial z = 0$), no shear stress at the fluid-air interface [$\tau_{rz}(r_1 + h) = 0$], and no yielding at the rod-fluid interface [$\tau_{rz}(r_1) \geq -\tau_c$].

[29] L. Jørgensen, M. Le Merrer, H. Delanoë-Ayari, and C. Barentin, Soft Matter **11**, 5111 (2015).